https://doi.org/10.15407/ufm.21.04.499

O.V. BYAKOVA[1], A.O. VLASOV[1,*], O.A. SCHERETSKIY[2], and O.I. YURKOVA[3,]**

[1] I.M. Frantsevich Institute for Problems in Materials Science of the N.A.S. of Ukraine, 3 Academician Krzhizhanovsky Str., UA-03142 Kyiv, Ukraine
[2] Physical-Technological Institute of Metals and Alloys of the N.A.S. of Ukraine, 34/1 Academician Vernadsky Blvd., UA-03142 Kyiv, Ukraine
[3] National Technical University of Ukraine 'Igor Sikorsky Kyiv Polytechnic Institute', 37 Prospect Peremohy, UA-03056 Kyiv, Ukraine

* La_04@ukr.net, ** yurkova@iff.kpi.ua

THE ROLE OF TECHNOLOGICAL PROCESS IN STRUCTURAL PERFORMANCES OF QUASI-CRYSTALLINE Al–Fe–Cr ALLOY

The present study emphasizes the role of processing strategy in terms of its effect on structural performances, heat-treatment response, and mechanical behaviour of quasi-crystalline Al–Fe–Cr-based alloy with nominal composition $Al_{94}Fe_3Cr_3$. Several kinds of semi-products and bulk-shaped materials, all processed with $Al_{94}Fe_3Cr_3$ alloy, have been produced using rapid solidification by melt spinning, powder atomization, hot extrusion, and cold-spraying, respectively. All kinds of semi-products and bulk-shaped materials comprised nanosize quasi-crystalline particles of *i*-phase, all embedded in α-Al matrix, although fraction volume of quasi-crystals and other structural parameters were rather different and dependent on processing route. In particular, cold-spraying technique was believed to give essential advantage in retaining quasi-crystalline particles contained by feedstock powder as compared to currently employed hot extrusion. Crucial role of nanosize quasi-crystalline particles in structural performances and superior combination of high strength and sufficient ductility of ternary Al–Fe–Cr alloy was justified over evolution of mechanical properties under heating. In this aim, evolution of the structure and mechanical properties of each kind of $Al_{94}Fe_3Cr_3$ alloy in response to heat treatment was examined and discussed by considering the classical strengthening mechanisms. A set of mechanical characteristics including microhardness, *HV*, yield stress, σ_y, Young's modulus, *E*, and plasticity characteristic δ_H/δ_A was determined by indentation technique and used in consideration. Strength properties (*HV*, σ_y, *E*) and plasticity characteristic (δ_H/δ_A) of cold-sprayed $Al_{94}Fe_3Cr_3$ alloy were revealed to be much high-

Citation: O.V. Byakova, A.O. Vlasov, O.A. Scheretskiy, and O.I. Yurkova, The Role of Technological Process in Structural Performances of Quasi-Crystalline Al–Fe–Cr Alloy, *Progress in Physics of Metals*, **21**, No. 4: 499–526 (2020)

er than those provided by currently employed hot extrusion. The important point concerns the fact that cold-sprayed $Al_{94}Fe_3Cr_3$ alloy kept almost stable values of mechanical properties at least up to 350 °C, suggesting potential application of this material in engineering practice under intermediate temperature.

Keywords: quasi-crystals, aluminium alloy, melt spinning, powder atomization, cold gas-dynamic spraying, microstructure, mechanical properties.

1. Introduction

Quasi-crystalline Al-based alloys are presently ascribed to the so-called family of complex metallic alloys (CMAs), which are characterized by a complex crystallographic structure [1–3]. Among the other CMAs, Al-based alloys containing quasi-crystals and related crystalline compounds are especially of growing attention for researches employed in scientific and engineering applications. Quasi-crystals as a new class of solids were firstly discovered in rapidly solidified Al–Mn alloys by D. Shechtman *et al*. over 30 years ago [4, 5]. A few years later, the formation of quasi-crystals in Al–Mn alloy was also reported in Ref. [6]. Moreover, the formation of quasi-crystals in ternary Al-based systems containing Fe and Cu, or Pd and Mn, or Ni and Co was pointed out by Tsai *et al*. [7, 8]. At the present, metastable and stable quasi-crystals were revealed in more than a hundred ternary and higher order alloys [9, 10]. A number of books, reviews, and papers concentrated attention on structural aspects of quasi-crystals, which are nowadays attributed to CMAs. In these publications, it has been reported that quasi-crystals exhibit a lattice with no periodicity anymore in the usual 3-dimensional space [3–6, 11–13]. Generally, the quasi-crystals show long-rang transitional order, quasi-periodicity, and a non-crystallographic orientational order, which are associated with the classically forbidden fivefold (icosahedral), 8-fold (octagonal), 10-fold (decagonal), and 12-fold (dodecagonal) symmetry axis [9]. Besides unusual aperiodic atomic structure, quasi-crystalline solids exhibit a remarkable combination of unique and sometimes unexpected physical, chemical, and mechanical properties, *i.e.* low density, high hardness, strength and elastic modulus, low surface energies and friction coefficient; good resistance to wear and corrosion, *etc*. [3, 9, 14–19]. Unfortunately, quasi-crystals are generally too brittle to be used in engineering practice as monolithic material [3, 17]. For comparison, Vickers hardness of quasi-crystals ranging from 7.8 to 9.5 GPa is very closed to hardness values for steels, which are usually ranged from 1.8 to 7.7 GPa [12, 17]. On the other hand, fracture toughness, K_{Ic}, of Al–Co–Cu–Si quasi-crystals is about 1.0–1.5 MPa $\cdot$ m$^{1/2}$ [17] while that for Al–Cu–Fe–B quasi-crystalline films was found to be between 1.5 and 1.9 MPa $\cdot$ m$^{1/2}$ [20]. The latter values of the K_{Ic} are very close to the value of K_{1c} for technical glass, which can be estimated as small as

K_{Ic} = 1.17 MPa · m$^{1/2}$. Despite of brittle nature of quasi-crystals, their outstanding properties was proved in design of low friction and/or wear and corrosion resistant coatings [1, 15, 16, 20–23]. Besides thermal and plasma spraying techniques, both used in processes with atomized powders, physical vapour deposition (PVD) [24] and chemical vapour deposition (CVD) [25] were applied for creation of quasi-crystalline surface layers. On the other hand, CMAs with composite structure comprising quasi-crystalline phase dispersed over Al matrix are capable to reduce the problem associated with brittle behaviour of bulk material [3, 26–28]. The same was believed to be true for Al-based composite coatings, which exhibit valuable properties of the incorporated quasi-crystalline phase [29–33].

In line with this, Al-based CMAs, which contain Al-rich quasi-crystals being alloyed with some other metals (like Fe, Cr, Cu or Pd, Mn, or Co, Ni, *etc*.), are thought to have the best potential for engineering practice [1, 3, 26, 27]. Actually, Al-based CMAs reinforced by nanosize quasi-crystals of *i*-phase offer undisputable advantages related to reasonable combination of high strength and sufficient ductility [27, 34–40]. Among the other CMAs, the attention is primary focused on those containing quasi-crystals of Al alloyed with Fe, Cu or Cr dispersed over Al-matrix [41–44]. In spite of industrial application of the above, the Al-based CMAs remains rather limited with intention to be potentially useful at a manufacturing production rate. In particular, reduced adhesion indicative of Al–Cu–Fe quasi-crystals [45] was used to develop a commercially produced Al–Cu–Fe–Cr quasi-crystalline coatings for cookware [46], while their low surface energy was recently found to prove design of self-lubricating, low-friction, wear-resistant Al–Cu–Fe–B coating [47]. In addition, Al–Cu–Fe quasi-crystalline CMAs can be used in design of solar light absorbers owing to high absorption of infrared light [3, 48].

High elevated-temperature strength being ensured by increased structural stability was believed to be distinctive feature of ternary and higher order Al–Fe–Cr-based nano-quasi-crystalline alloys, making them attractive for potential industrial application and, especially, for that in aircraft industry [28, 34, 35, 37, 38, 42, 49, 50]. The same as it was reported for that based on Al–Cu–Fe alloys, composite structure consisted of α-Al matrix reinforced by nanosize quasi-crystals of *i*-phase is intrinsic of CMAs based on Al–Fe–Cr system [26, 37, 39, 50–52]. Of importance is excellent balance between a high strength and sufficient ductility of Al–Fe–Cr-based quasi-crystalline alloys [35–38, 40, 49, 53] compared to commercial Al-based alloys recommended for service under elevated temperature. In addition, Al–Fe–Cr/Al–Cu–Fe–Cr-based CMAs are considered to be interesting because of high stability in a broad pH range [54–58]. Presently Al–Fe–Cr-based CMAs are employed as rein-

forcement filler intended for wear resistance enhancement of Ti metal matrix composites and coatings [41, 59, 60].

Generally, rapid solidification technique with high cooling rate about 10^5 K/s is required to create quasi-crystalline phases [28, 61, 62]. After the initial discovery of quasi-crystals in rapidly-cooled Al-alloys Al–Mn alloy [4] the above solids were found in Al-based CMAs alloyed by Fe, Cr, V, Ti, Zr, Nb, and Ta [35–37, 39, 49, 51]. A number of various processes involving different routes and techniques, which are capable for creation of Al-based quasi-crystalline alloys, have been developed during the last years [63–67]. However, the rapid solidification by melt spinning [27, 36, 39, 50, 51, 68] and powder atomisation technique performed with either argon-gas [28] or inhibited water [37, 40] are thought to be mostly effective for mass production. Thus, the nano-quasi-crystalline Al-based alloys are generally performed as semi-products in form of either melt-spun ribbons/flakes [36, 38, 39] or gas/water atomised powders [35, 37, 52]. Because of this, the development of processing routes available for semi-product consolidation is of great importance for manufacturing the bulk-shaped material and, consequently, further improvement of structural stability is desirable to maximize elevated temperature. Presently, the hot extrusion [27, 34, 37, 49, 52, 69], spark plasma sintering [70], spray forming [67], and cold spraying technique [71, 72] as alternative process are developed to consolidate quasi-crystalline semi-product in bulk shaped material.

In this paper, we overview the previous findings by the authors and some new results, which highlight the role of processing route in structural performance of semi-products such as melt-spun ribbon and atomised powder as well as bulk-shaped materials in form of extruded rod and cold-sprayed coating. All of the above materials were performed with quasi-crystalline Al–Fe–Cr alloy and investigated by x-ray diffraction analysis (XRD), electron microscopy (SEM and TEM modes), and differential scanning calorimetry (DSC).

2. Materials and Methods

2.1. Materials and Processing

Quasi-crystalline alloy with nominal composition $Al_{94}Fe_3Cr_3$ was used in experiments. Quasi-crystalline semi-products materials were performed in form of rapidly solidified ribbons and water atomized powder. Rapidly solidified ribbons were produced by melt spinning under a reduced argon atmosphere and cooper wheel speed of 40 m/s. Arc-melted ingots of Al alloyed by proper content of Fe and Cr were explored in preparing of melt-spun ribbons. So that, as-quenched ribbons with thickness ranged between 20 and 30 μm and width roughly about 8 mm were prepared under cooling rate of 10^6 K/s. Quasi-crystalline powder of Al-based al-

loy with nominal composition of $Al_{94}Fe_3Cr_3$ and oxygen content about 0.2% was fabricated by water-atomization technique using inhibited high-pressure water with pH 3.5 [73]. As compared to conventional gas-atomisation process, water-atomization technique provides for high cooling rates up to 10^6 K/s although the oxygen content was almost the same. After atomization, the powder particles were sieved to less than 40 μm in size using the corresponding sieves. Fraction volume of quasi-crystalline particles contained by powder was not higher than 30% [37].

Consolidation of quasi-crystalline powder was performed by two different techniques, *i.e.* by hot extrusion process and cold sprayed technique. So, extruded rods and thick coatings were obtained as bulk shaped materials. Consolidation of quasi-crystalline powder *via* hot extrusion process was done in hermetic capsule at the temperature of 380 °C [37]. Prior to extrusion, capsule of 25 mm in diameter filled by pre-compacted powder was degassed at the temperature of 350 °C during 1 hour. Press of 125000 kg in power and equipped by extrusion die with inner diameter, d_e = 8 mm and length of working part about l_e = 2 mm was used in extrusion process. Extrusion was performed in a single pass with reduction coefficient k_e = 9.8. Extrusion parameters such as longitudinal pressure of P_l = 1.1 GPa and extrusion velocity of $V_e = 15 \cdot 10^{-3}$ m/s were employed in experiments.

Commercial cold-spray system (DYMET 403) was used in spraying experiments with compressed air. Cold-sprayed principle and technical set-up for cold spraying are described elsewhere [72, 74]. Velocity of air/particle jet was roughly about V = 750 m/s while its temperature was as high as 400 °C [71]. The detailed description of cold spraying conditions was reported in [71]. Cold rolled plates of low carbon steel (carbon content 0.2%) with a thickness about 3.0 mm were used as substrates, which were sandblasted prior to spraying. Finally, samples of coatings with thickness about 800 μm were obtained for further experiments.

2.2. Structural Characterization

Structural characterisation of melt-spun alloy, water atomized powder, cold-sprayed alloy and as-extruded rod was performed by x-ray diffraction (XRD) analysis using Cu K_α radiation. The quasi-crystalline *i*-phase was indexed by using Cahn's indexation scheme [75].

Scanning and transmission electron microscopy (SEM and TEM) was used to obtain basic information concerning microstructural features of semi-products and consolidated materials including quasi-crystalline particles morphology (size and shape). Electron microscope Jeol Superprobe-733 (JEOL, Japan) equipped with x-ray detectors (EDX and EPMA) was used to get SEM images while JEM 2100 F (JEOL, Japan)

microscope was employed to obtained TEM images and selected areas of electron diffraction (SAED) patterns as well.

Prior to SEM observation feedstock powder was glued by conductive compound to plate for preparing a slice by standard metallographic technique with polishing by diamond slurry. The same polishing procedures were used to prepare surface and cross-sections of pieces being cut off extruded rods and coatings.

Differential scanning calorimetry (DSC) was employed to study structural stability of semi-products and consolidated materials under elevated temperatures. DSC/TGA measurements were performed by using STA449F1 analyser (Netzsch, Germany). Each kind of the sample was placed into DSC cell and exposed under argon flow rate about 20 ml/min during continuous heating from room temperature up to 893 K. Heating rate used in DSC/TGA measurements was as great as 10 K/min.

2.3. Mechanical Testing

Microhardness measurements were performed using a conventional microhardness machine equipped by standard Vickers pyramid. Microhardness numbers were determined under indentation loads not higher than 1.0 N. Yield stress, σ_y, was extracted from 'stress–strain' curves constructed by a set of trihedral pyramids with different angles at the tip γ_1 (ranged from 45° to 85°) according to the test method procedure [76].

Plasticity characteristic δ_H as dimensionless parameter that may vary in the range from 0 (for 'pure' elastic contact) to 1 (for 'pure' plastic contact) was derived by calculations through microhardness, HV, and Young's modulus, E [77]. Following equation was used for calculation of plasticity characteristic δ_H through Vickers hardness [77]:

$$\delta_H = 1 - 14.3\left(1 - \nu - 2\nu^2\right)\frac{HV}{E}, \qquad (1)$$

where ν and E are respectively Poison's ratio and Young's modulus of tested material.

Microtester capable for load-displacement measurements and equipped by trihedral Berkovich pyramid was used to determine Young's modulus, E, according to the test method procedure originally proposed by Oliver and Pharr [78].

In addition, plasticity characteristic δ_A, which is physically close to that denoted by δ_H, was derived from loading and unloading data according to the demands of International Standard ISO 14577-1:2002. Principles and test method procedure accepted for determination the plasticity characteristic δ_A, are described in [79, 80]. Of importance is that no evidences concerning the values of Young's modulus, E, and Poison ratio, ν, are not required for determination of plasticity characteristic δ_A compared to calculation of δ_H parameter according equation (1).

3. Results and Discussion

3.1. Structural Characterisation of Quasi-Crystalline Semi-Products

SEM images of microstructure of as-received melt-spun ribbons and as-atomised powder demonstrate a huge numbers of white particles presented in the rapidly solidified alloy and interior of the powder particles, as shown in Fig. 1.

The results of XRD analysis indicate quasi-crystalline nature of melt-spun alloy and atomized powder, see Fig. 2, *a*, *b*. XRD patterns recorded for the semi-products indicate the presence of icosahedral phase (*i*-phase) indexed using Cahn's indexation scheme [75] besides α-Al indexed with reflections corresponding to (111), (200), (220), and (311) planes in the range of 2θ between 30 and 85°.

The results of XRD analysis were found to be in accordance with data obtained by TEM observation. Figure 3 displays representative bright field TEM images for the melt-spun alloy, which shows quasi-crystalline particles embedded in α-Al matrix. Five-fold reflection spots

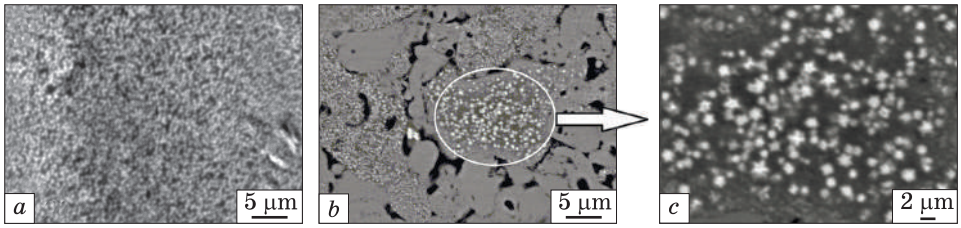

Fig. 1. SEM images of microstructure for (*a*) as-received melt-spun ribbons and (*b*, *c*) as-atomised powder

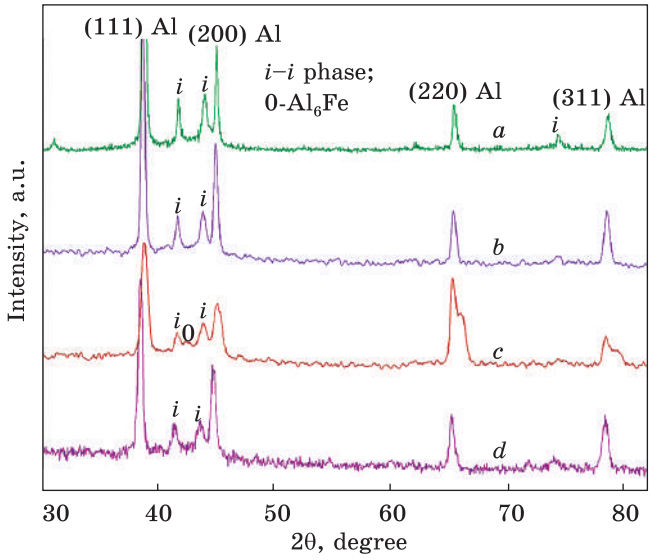

Fig. 2. XRD patterns of *a* — as-spun alloy, *b* — water atomized powder, *c* — extruded sample, and *d* — as-sprayed coating; all performed with $Al_{94}Fe_3Cr_3$ alloy [72]

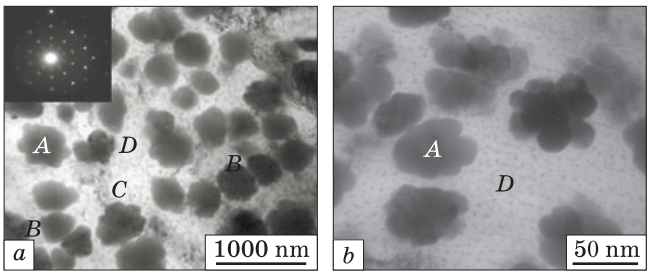

Fig. 3. Bright-field TEM images showing the microstructure of as-spun alloy of different magnification (*a*, *b*): *A* — rounded quasi-crystalline particles; *B* — rosette-like quasi-crystalline particles; *C* — grain boundary precipitates; *D* — fine crystalline particles inside the α-Al grains. In (*a*), the SAED pattern corresponded to a single quasi-crystalline particle (at the upper left-hand corner)

indicative of *i*-phase are revealed in SAED pattern, as can be seen in Fig. 3, *a* originally published in [72]. Quasi-crystalline particles of rounded (*A*) and/or rosette-like (*B*) shape with the size around 300 nm are presented in α-Al matrix, as evidenced from Fig. 3, *a*. However, scattering of fine quasi-crystals of rounded shape and size ranged from 20 to 50 nm are also found, as can be seen in Fig. 3, *b*. These kinds of icosahedral quasi-crystalline particles have been observed by other authors [36, 39, 50]. In the atomized powder, quasi-crystalline particles with the size increased up to 1.5 μm are also revealed, suggesting variable cooling conditions for water jets, as shown in Fig. 1, *b*, *c*.

Characteristic feature of microstructure for the melt-spun alloy is the presence of grain boundary precipitates and very small particles placed inside the α-Al grains, as can be seen in Fig. 3. The latter were identified as those corresponded to metastable crystalline phases, *i.e.* distorted multiphase θ-$Al_{13}(Fe,Cr)_{2-4}$ and/or Al_6Fe [39, 50, 68].

3.2. Structural Characterization of Bulk-Shaped Quasi-Crystalline Material

Figure 4 demonstrates SEM images for the microstructure of as-received extruded rod and as-sprayed coatings, both performed by using feedstock quasi-crystalline powder.

It can be seen in Fig. 4 that severe plastic deformation indicative of extrusion process and cold-spraying technique is quite enough to break off the oxide film presented always on the surface of Al-based particles and provided for their intimate metallurgical bonding.

However, morphology of powder particles observed in deformation-induced structure of extruded rod and cold-sprayed coating is rather different. Powder particle elongated in parallel to extrusion direction are created in the cross-sectional microstructure of extruded rod whereas flattened and heavily deformed particles are formed in the cross-sectional microstructure of cold-sprayed coating. Thus, extrusion process results in formation of elongated rod-shaped powder particles with

aspect ratio the same as reduced coefficient $k_e = 9.8$ while cold spraying compels feedstock particles to get elongated lens-like shape with aspect ratio $k_f \approx 4.7$. Processing conditions are responsible for difference of structural features observed in extruded rod and those indicative of cold-sprayed coating. Deformation of feedstock powder at extrusion is controlled by bar drawing being operated by two components of pressure such as longitudinal, P_l, and transversal one, P_t. By adopting longitudinal pressure P_l (1.1 GPa) used in the experiments, and geometrical parameters ($l_e = 2$ mm, $d_e = 8$ mm) for working part of extrusion die, transversal pressure can be estimated as great as $P_t = 2.2$ GPa. Taking into consideration the extrusion velocity used in experiments ($V_e = 15 \cdot 10^{-3}$ m/s) and geometrical parameter of extrusion die ($l_e = 2$ mm) it is easy to show that two components of pressure operate the extruded sample as long as $\tau = 1.3 \cdot 10^{-1}$ s.

As opposed to extrusion process, consolidation of feedstock powder in coating is mainly controlled by forward pressure. The latter is defined by air/particle jet and it can be assessed as great as $P_f \approx 1.9$ GPa at the conditions accepted in the present study. In practice, high value of forward pressure results in severe plastic deformation of powder particles, suggesting flattening and mechanical interlocking the splats by cold forging. However, adiabatic shear instability under high strain rate resulted from high impact velocity is primary responsible for effective metallic bonding between the adjacent particles [81–86]. High value of forward pressure and very short contact time of impact about 10^{-8} s [85, 86], favours particle surface softening and shear localisation. This bonding process is commonly considered as that comparable with explosive welding or shock wave powder compaction [87]. Figure 4, *b* shows the evidences of strong shear localisation including those indicative of metallurgical bonding by impact fusion.

Despite of severe plastic deformation of material under extrusion process and cold spraying, huge number of quasi-crystalline particles of almost unchanged shape survives inside heavily deformed feedstock powder particles, as can be seen in Fig. 4. The results of XRD analysis confirm the presence of quasi-crystalline particles in α-Al matrix, as can be seen in Fig. 2. However, there are few differences of XRD patterns for the as-extruded sample and the as-sprayed coating compared

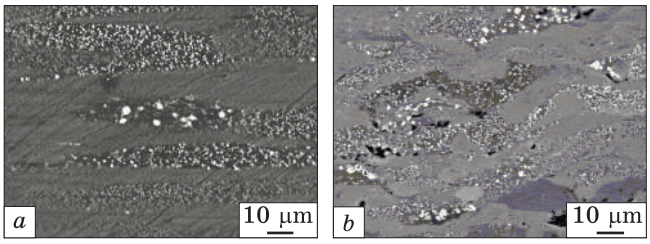

Fig. 4. Cross-sectional microstructures of (*a*) as-extruded rod arranged parallel to extrusion direction and (*b*) as-sprayed coating

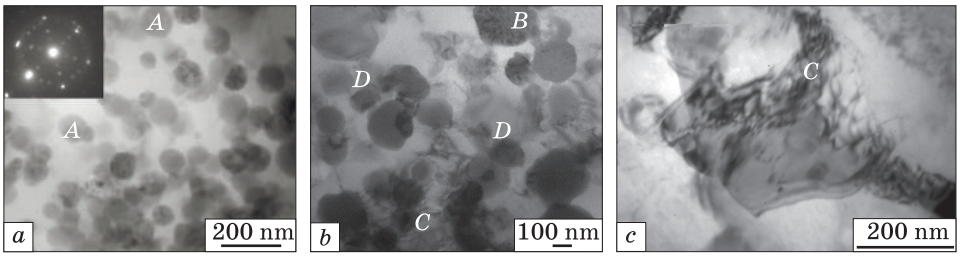

Fig. 5. Bright-field TEM images showing the microstructure for as-extruded sample of $Al_{94}Fe_3Cr_3$ alloy of different magnification (*a*, *b*, *c*): *A* — rounded quasi-crystalline particles; *B* — rosette-like quasi-crystalline particles; *C* — dislocation tangle; *D* — crystalline particles of rectangular shape. In (*a*), SAED pattern corresponded to a single quasi-crystalline particle (at the upper left-hand corner)

to those for the as-spun alloy and the as-received atomised powder. Compared to feedstock atomized powder, intensity of icosahedral reflections presented in XRD pattern for the as-extruded samples is much lesser, suggesting reduced fraction volume of quasi-crystalline phase, as can be seen in Fig. 2, *c*. The above evidence allows us to assume that quasi-crystalline particles would be partially decomposed under the combined effect of high pressure and enhanced temperature during hot extrusion process. Actually, weak XRD peak at $2\theta \approx 42.1°$ corresponding to the metastable Al_6Fe phase is observed in the XRD pattern of the as-extruded sample. Moreover, there are additional reflections of α-Al overlapping with those from α-Al typical for the feedstock powder, indicating the formation of two α-Al solid solutions with different elementary composition. As it is evidenced from data listed in Table 1, one of the α-Al solid solutions has lattice parameter a_0, which is almost the same as that for the as-atomized feedstock powder. Another α-Al solid solution demonstrates reduced lattice parameter a_0, suggesting the enrichment of α-Al by dissolved Fe and Cr, which atomic radii are smaller by ≈12% than the atomic radius of Al.

In addition, reflections of α-Al presented in XRD pattern for the as-extruded rod are found to be broad, suggesting dislocation activity. The results listed in Table 1 show that dislocation density recorded in α-Al

Table 1. **Parameters of elements and α-Al solid solutions in $Al_{94}Fe_3Cr_3$ alloy performed *via* different processing routes**

Parameters	Al	Fe	Cr	Melt-spun alloy	Atomized powder	Extruded material	Cold-sprayed alloy
Lattice parameter a_0, nm	0.4050	0.2866	0.2884	0.4037	0,4042	0.4043 (0.4011)	0.4045
Dislocation density ρ, m/m^3	—	—	—	10^{11}	10^{13}	10^{16}	10^{15}

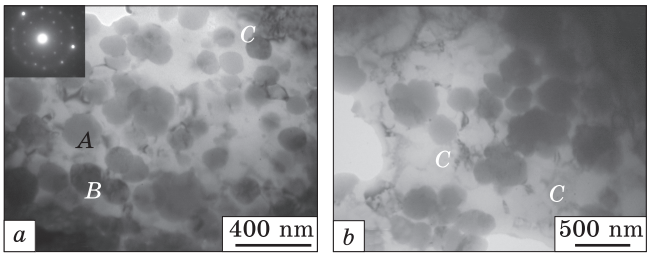

Fig. 6. Bright-field TEM images showing the microstructure of as-sprayed alloy (*a*, *b*): *A* — rounded quasi-crystalline particles; *B* — rosette-like quasi-crystalline particles; *C* — dislocation tangle. In (*a*), SAED pattern corresponded to a single quasi-crystalline particle (at the upper left-hand corner)

solid solution of extruded material achieves the value $\rho = 10^{16}$ m/m^3, which exceeds by 3-order magnitude that recorded for feedstock atomized powder.

The data of TEM observation are in good agreement with the results determined by XRD analysis. Quasi-crystalline particles, which have rounded (A) and/or rosette-like (B) shape and size ranged from 50 to 300 nm, are visible in α-Al matrix of as-extruded material, as can be seen in Fig. 5, *a*, *b*. In addition, a few crystals (D) with rectangular shape, which could be presumably corresponded to Al_6Fe phase, and dislocation tangles (C) are also visible in the microstructure of the as-extruded material, as can be seen in Fig. 5, *b*, *c*.

No evidence referred to the presence of additional phases besides those corresponding to quasi-crystalline *i*-phase and α-Al is found in the XRD pattern of as-received cold-sprayed alloy, as can be seen in Figure 2, *d*. This result is in good agreement with the data published previously for cold-sprayed coatings although they were deposited at the temperature smaller than that used in the present study [71]. It is noticeable that the all reflections corresponding to α-Al shift towards smaller 2θ compared to those recorded in the XRD pattern of the as-atomized powder. This fact indicates the increase of lattice parameter a_0 of α-Al solid solution of the as-received cold-sprayed alloy and, thus, its depletion by dissolved Fe and Cr. Actually, lattice parameter a_0 of α-Al solid solution for the as-received cold-sprayed alloy shows the greatest value compared to other products, as evidenced from the data listed in Table 1. In addition, dislocation density recorded in α-Al solid solution of the as-received cold-sprayed alloy much superior to that of semi-products although it is smaller by order magnitude than that of the as-extruded material, as can be seen in Table 1. Figure 6 shows bright-field images of microstructure for as-received cold-sprayed alloy. It can be seen that microstructure of the as-received cold-sprayed alloy is very similar to that of the as-extruded material. The difference is that quasi-crystalline particles visible in the microstructure of the as-received cold-sprayed alloy have rather bigger size than those presented in the

as-extruded material. In addition, no crystalline particles of rectangular shape are found in the microstructure of the as-sprayed alloy. Moreover, compared to the as-extruded material, fraction volume of dislocation tangles presented in α-Al matrix of the as-sprayed alloy is much less, as can be seen by comparison Fig. 6, *b* and 5, *b*. This is because of extremely short time of particle/particle interaction by impact.

3.3. The Effect of Processing Route on Thermal Stability of Quasi-Crystalline Al–Fe–Cr Alloy

Figure 7 shows DSC runs for investigated samples originally published in [72]. Several exothermic peaks detected by DSC measurements are originated from basic processes ascribed to phase and structural transformations, which occur in microstructure of quasi-crystalline material at heating.

The main exothermic peak *B* is commonly associated with the process, which involves gradual dissolution of the quasi-crystalline particles together with simultaneous formation of more stable crystalline Al_6Fe particles and stable intermetallic compounds such as θ-$Al_{13}Fe_4$ and θ-$Al_{13}Cr_2$ [36, 39, 50, 51, 68, 88]. Attention should be paid to an additional exothermic peak *C* at the 480 °C overlapping with exothermic peak *B*, both observed in DSC run for the melt-spun alloy. Replacing of the metastable precipitates by more stable and large crystalline particles of the Al_6Fe and multiphase $Al_{13}(Fe,Cr)_{2-4}$ phases is thought to be the reason of exothermic reaction *C*. Figure 8 displays the microstructural evolution of the melt-spun alloy after heat treatment with holding time of 20 min at different temperatures, *i.e.* 350, 400, 450, and 500 °C.

It can be seen that the sample heat treated at 350 °C demonstrates microstructure similar to that of as-spun alloy, see Fig. 8, *a*. The differ-

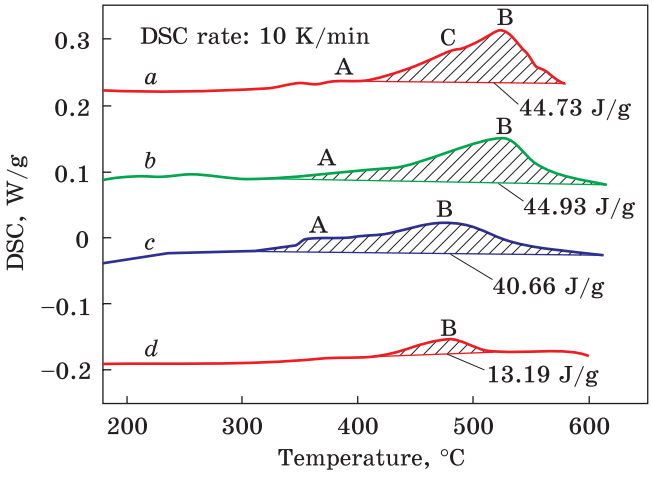

Fig. 7. DSC runs for (*a*) the melt-spun alloy, (*b*) atomized powder, (*c*) cold-sprayed alloy, and (*d*) extruded material [72]

ence is that some quasi-crystalline particles increase in size up to 500 nm compared to the as-spun alloy. After heat treatment at 400 °C, additional large particles with angular shape are formed in between rounded quasi-crystalline particles of reduced size, as can be seen in Fig. 8, *b*.

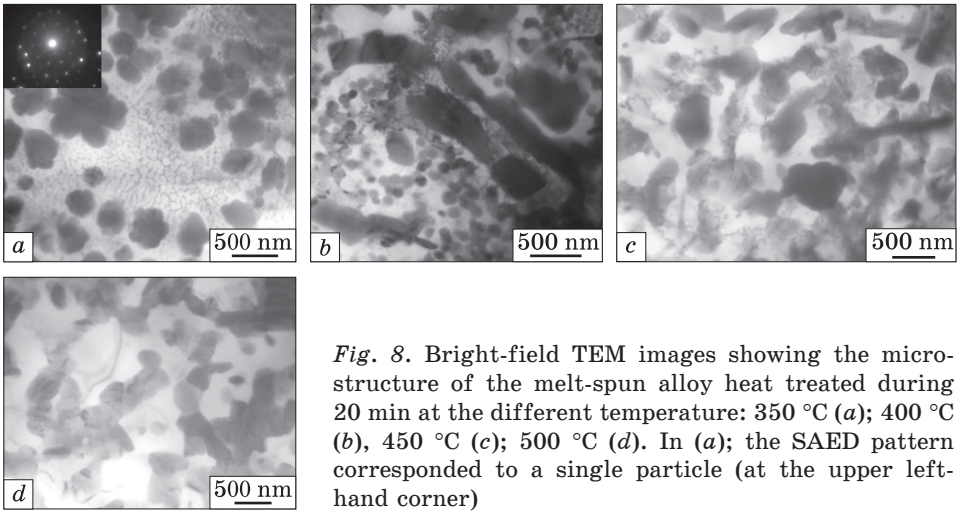

Fig. 8. Bright-field TEM images showing the microstructure of the melt-spun alloy heat treated during 20 min at the different temperature: 350 °C (*a*); 400 °C (*b*), 450 °C (*c*); 500 °C (*d*). In (*a*); the SAED pattern corresponded to a single particle (at the upper left-hand corner)

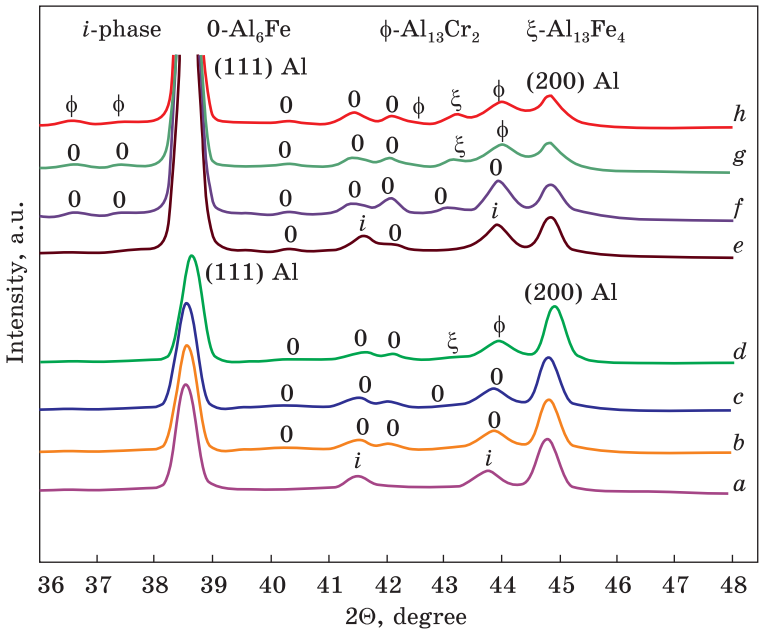

Fig. 9. XRD patterns of the (*a–d*) atomized powder and (*e–h*) melt-spun alloy, both heat treated during 20 min at different temperatures: 400 °C (*a*) and (*e*); 450 °C (*b*) and (*f*); 500 °C (*c*) and (*g*); 550 °C (*d*) and (*h*)

Disappearance of previously existing precipitates and quasi-crystalline particles with reduced size compared to that indicative of the as-spun alloy is important. Besides continuous dissolution of the quasi-crystalline particles, formation of large multiphase particles due to the growth of precipitates/small particles and their further transformation into more stable crystalline phase dominates structural evolution of the melt-spun alloy during annealing [68]. Course crystalline particles with angular and rod-like shapes are formed in microstructure of the samples heat-treated at 450 and 500 °C, as shown in Fig. 8, *c*, *d*.

The results of XRD analysis specify mention above. As evident in Fig. 9, quasi-crystalline particles survive in the microstructure of the melt-spun alloy at heating up to 400 °C despite of simultaneous formation of the metastable crystalline Al_6Fe-phase.

The latter remains in the modified microstructure of Al-based alloy heat treated up to 550 °C and transformed at least into the stable θ-$Al_{13}Fe_4$ and θ-$Al_{13}Cr_2$ phases at higher temperature.

It is noticeable that reflections corresponding to the metastable crystalline Al_6Fe-phase appear in XRD pattern of the atomized powder after heat treatment at the temperature higher by 50 °C than that of the melt-spun alloy, as can be seen in Fig. 9. This fact indicates that the presence of the ultrafine precipitates in the microstructure favours crystallization process occurred at heating of the melt-spun alloy. In addition, lattice parameter of α-Al solid solution for the melt-spun alloy superior to that for the atomized powder over the all range of heat treatment temperatures, suggesting the increased kinetic for the formation of crystalline phases. In addition, phase transformation of the melt-spun alloy at heating is going rather different from that of the atomized powder. Five meaningful stages of phase transformation could be assigned for the melt-spun alloy whereas only four stages are thought to be distinctive of the atomized powder, as shown in Fig. 10. In the melt-spun alloy, lattice parameter of α-Al solid solution increases gradually as the temperature of heat treatment increases up to 500 °C. This fact indicates depletion of α-Al matrix by dissolved Cr and Fe, which occurs due to the growth of some quasi-crystalline particles up to 500 nm after heat treatment at the 350 °C whereupon the all quasi-crystalline particles commence to dissolve progressively and the particles of more stable crystalline Al_6Fe phase is formed as ever the heat treatment temperature rises up to 450 °C. Further depletion of α-Al matrix by dissolved Cr and Fe occurs owing to the formation of additional particles of the stable θ-phases when the heat treatment temperature increases up to 500 °C. In the melt-spun alloy heat treated at the temperatures higher than 500 °C, lattice parameter of α-Al solid solution tends to somewhat decrease when the metastable Al_6Fe particles are completely replaced by the particles of stable θ-phases

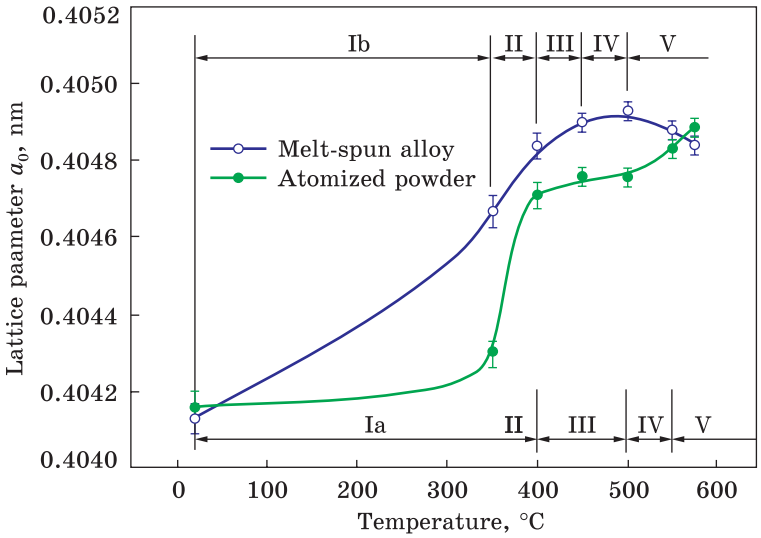

Fig. 10. Lattice parameter of α-Al solid solution *vs*. temperature of heat treatment used for the melt-spun alloy and atomized powder. Structural regions: Ia — α-Al + *i*-phase, Ib — α-Al + *i*-phase + nanosize precipitates θ-$Al_{13}(Fe,Cr)_{2–4}/Al_6Fe$, II — α-Al + *i*-phase + + Al_6Fe, III — α-Al + Al_6Fe, IV — α-Al + Al_6Fe + θ-phases, V — α-Al + θ-phases

and, particularly, preferably of the θ-$Al_{13}Cr_2$ phase, as evidenced from Fig. 9.

In the atomized powder, the increase of lattice parameter for α-Al solid solution in response to heat treatment at the temperatures less than 350 °C is insignificant, as can be seen in Fig. 10. However, lattice parameter for α-Al solid solution increases sharply just as the heat treatment temperature increases up to 400 °C, suggesting growth of the quasi-crystalline particles. Variation of lattice parameter for α-Al solid solution in response to heat treatment at the temperatures ranged from 400 to 500 °C is rather negligible. At this temperature conditions, the quasi-crystalline particles of *i*-phase are completely replaced by the more stable crystalline Al_6Fe phase, resulting in the modified microstructure. The increase of lattice parameter for α-Al solid solution occurs at the temperatures above 500 °C when particles of the stable θ-phases are formed. Finally, lattice parameter for α-Al solid solution of the atomized powder achieves the value almost the same as that of the melt-spun alloy heat-treated at the temperature of 575 °C.

The origin of broad exothermic peak *A* is thought to be rather different compared to that of exothermic peak *B*. By considering common knowledge, it is easy to show that the exothermic peak *A* arises from dislocation activity within α-Al matrix the same as for many other metals and alloys [89, 90]. In the general case, reorganization and recrystallization processes result in exothermic reactions. Actually, the value of

exothermic peak *A* good correlates with dislocation reorganization and recrystallization process. Excepting the extruded alloy, the value of heat flow for the exothermic reaction *A* increases as dislocation density in α-Al matrix increases, see Table 1. In particular, the greatest value of heat flow for the exothermic reaction *A* is indicative of the cold-sprayed alloy while the smallest value of heat flow for the same reaction is observed for the melt-spun alloy. Heat flow for the exothermic reaction *A* of the atomized powder is of intermediate value between those for the melt-spun and cold-sprayed alloys. Moreover, the exothermic reaction *A* attributed to the cold-sprayed alloy shifts toward lower temperature compared to that of the feedstock-atomized powder, as can be seen in Fig. 7. On the first glance, it is surprising that the exothermic peak *A* in DSC run of the extruded sample with the highest value of dislocation density within α-Al matrix is omitted. However, this phenomenon becomes understanding by considering the fact that recrystallization process would be realized during long-term pre-treatment at the 350 °C (see subsection 2.1).

A few aspects should be mentioned here as applied to structural stability provided by one or another processing route used in experiments for consolidation of the feedstock powder in bulk-shape material. First of all, attention should be paid to a shift of the main exothermic peak by about 50 °C toward lower temperature after the extrusion and cold-spraying processes, indicating an increased kinetic of the quasi-crystalline particles decomposition together with simultaneous formation of crystalline phases. Dislocation activity in α-Al matrix can largely facilitates dissolution of alloying elements released from decomposed metastable quasi-crystalline particles. The next aspect concerns the fact that consolidation of the feedstock powder in bulk-shaped material results in a reduction of the main exothermic peak *B*. However, diminution of the exothermic peak *B* for the cold-sprayed material is insignificant whereas that for the extruded alloy was found to be great. In cold-spraying process, particle/particle interaction is adiabatic due to ultra-short time of impact when heat conduction can be neglected [86]. As a result, adiabatic regime can lead to considerable overheating particle boundary and dissolution of some quasi-crystals located at the particle/particle interface while the other quasi-crystals placed inside powder particles remain intact.

The latter is thought to be in good agreement with the results of XRD analysis which show increased lattice parameter, a_0, and, so, depletion of α-Al matrix by dissolved Fe and Cr. Another one was believed to be true for the extruded alloy. Long-term pre-treatment at elevated temperature, which is followed by hot extrusion, favours partial decomposition of the quasi-crystalline particles and even creation of some amount of the crystalline metastable Al_6Fe-phase.

3.4. Correlation of Mechanical Properties and Structure of Al–Fe–Cr-Based Alloy

Mechanical characteristics including microhardness, *HV*, yield stress, σ_y, and plasticity characteristic δ_H/δ_A, of the melt-spun alloy, extruded material, and cold-spray coating, all performed *vs*. the heat treatment temperature, *T*, are shown in Figs. 11 and 12.

A few aspects could be mentioned here to clarify the role of processing route in term of its effect on structural stability and, hence, mechanical properties for $Al_{94}Fe_3Cr_3$-alloy. First of all, it can be seen that shape of 'σ_y–*T*' curves determined for all materials are very similar to those of '*HV*–*T*' ones [72], indicating the accuracy of measurement results. The fact is important that microhardness, *HV*, and yield stress, σ_y, decrease as heat treatment temperature, *T*, increases whereas plasticity characteristic δ_H/δ_A get higher values, as can be seen in Figs. 11, 12.

Several structural regions, which are similar to those used in Fig. 10, could be marked out in the above curves, as shown in Fig. 11, 12. In the initial regions I and II, the microhardness, *HV*, and the yield stress, σ_y, for the melt-spun alloy and the cold-spray coating decrease slightly whereas those for the extruded material keep almost stable values. In the region III, the increase of heat treatment temperature causes the values of microhardness, *HV*, and yield stress, σ_y, to reduce down stronger. In the last regions IV and V, the values of the above mechanical parameters decrease dramatically as the heat treatment temperature tends to increase up to 600 °C. It is worthy of note that microhardness, *HV*, and yield stress, σ_y, of the cold-sprayed coating superior to those of the melt-spun alloy and, especially, to that of the extruded material, all performed after heat treatment over the all range of temperatures.

Several aspects could be mentioned here to clarify the role of the microstructure and, in turn, processing route in mechanical properties of different kinds of $Al_{94}Fe_3Cr_3$ alloy, all performed before and after heat treatment. Combination of classical strengthening mechanisms is primary responsible for variation of strength properties. As applied to the subject matter, strength properties of the $Al_{94}Fe_3Cr_3$ alloy are mainly controlled by strengthening mechanisms such as follow: (i) content of alloying elements in α-Al matrix; (ii) strain hardening; (iii) the size and fraction volume of quasi-crystalline particles.

There are distinctive examples illustrating the effect of strengthening mechanisms on mechanical response of the $Al_{94}Fe_3Cr_3$-alloy. In particular, strength properties take the values as high as possible if and only if α-Al matrix is reinforced by quasi-crystalline particles. Strength properties are reduced with dissolution of quasi-crystals together with simultaneous formation of the metastable Al_6Fe particles and, especially, the particles of stable θ-phases, as can be seen in Fig. 11. Degrada-

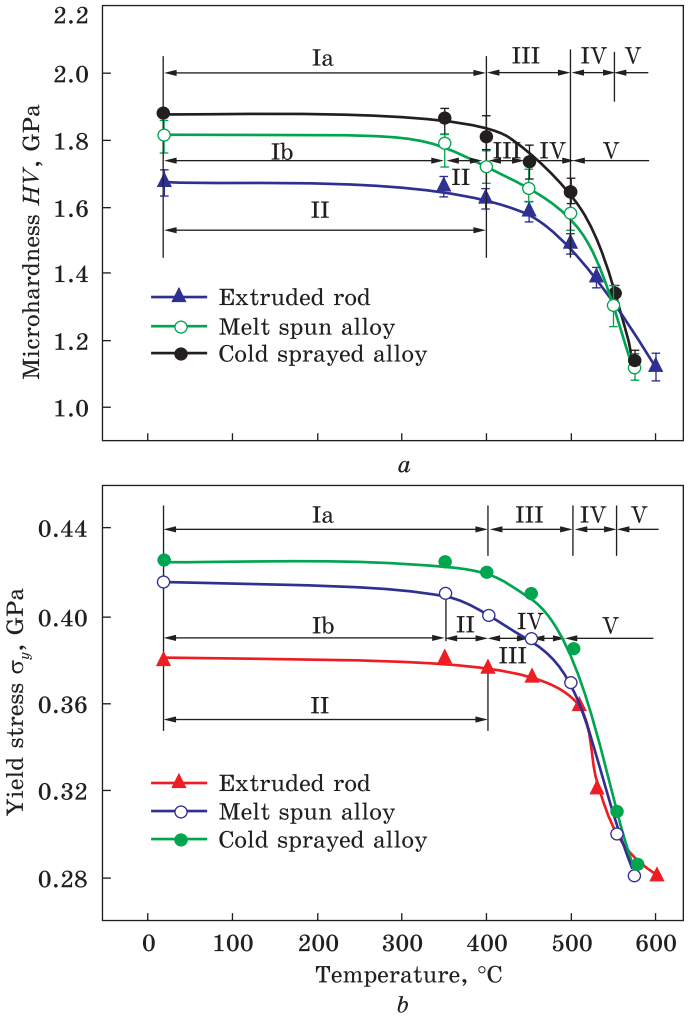

Fig. 11. The (*a*) microhardness, *HV*, and (*b*) yield stress, σ_y, *vs*. temperature used for heat treatment of melt-spun alloy, extruded material, and cold-spray coating. Structural regions: Ia — α-Al + *i*-phase, Ib — α-Al + *i*-phase + nanosize precipitates θ-$Al_{13}(Fe,Cr)_{2-4}$/Al_6Fe, II — α-Al + *i*-phase + Al_6Fe, III — α-Al + Al_6Fe, IV — α-Al + + Al_6Fe + θ-phases, V — α-Al + θ-phases. The data for microhardness (*a*) agree with those in Ref. [72]

tion of strength properties becomes stronger with depletion of α-Al matrix by solute Fe and Cr, as shown in Fig. 10.

In addition, strength characteristics are so much higher as fraction volume of the quasi-crystalline particles is greater. It becomes clear, at the most, by comparison of the microstructural characteristics and mechanical properties for the cold-sprayed alloy and the extruded material, as it is evidenced from the data presented in Figs. 7, 11.

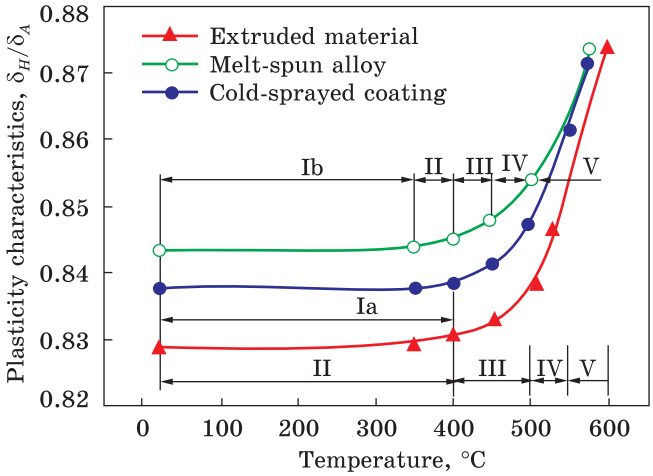

Fig. 12. The data for plasticity characteristics δ_H/δ_A plotted *vs.* the temperature used for heat treatment of the melt-spun alloy, extruded material, and cold-spray coating. Structural regions: Ia — α-Al + *i*-phase; Ib — α-Al + + *i*-phase + nanosize precipitates θ-$Al_{13}(Fe,Cr)_{2-4}$/Al_6Fe; II — α-Al + *i*-phase + Al_6Fe; III — α-Al + + Al_6Fe; IV — α-Al + + Al_6Fe + θ-phases; V — α-Al + θ-phases

Moreover, extremely high dislocation density about 10^{15} m/m^3 resulted from strain hardening contributes directly in microhardness, *HV*, and yield stress, σ_y, of the cold-sprayed alloy, making its strength higher than that of the melt-spun alloy. Softening of the cold-sprayed alloy with increasing of the heat treatment temperature from 300 to 400 °C could be attributed to dislocation reorganization and recrystallization process resulted usually from annealing. Besides this, softening of the melt-spun alloy is rather related to depletion of α-Al matrix by solute Fe and Cr. This occurs either owing to quasi-crystals coarsening after heat treatment at 350 °C or due to quasi-crystals dissolution together with the formation of coarse crystalline particles of the more stable Al_6Fe phase after heat treatment at the temperature of 400 °C, as can be seen in Figs. 7–9. Stable values of microhardness, *HV*, and yield stress, σ_y, for the extruded material heat treated up to 400 °C is explained by the absence of recrystallization process that was realized during high temperature pre-treatment prior extrusion.

The next aspect concerns ductility of the $Al_{94}Fe_3Cr_3$ alloy. It is commonly supposed that material ductility increases as microhardness decreases. Actually, plasticity characteristic δ_H/δ_A for the melt-spun alloy get higher values compared to the cold-sprayed alloy whose microhardness, *HV*, is larger. From the above viewpoint it is surprising for the

Table 2. **Young's modulus for different kinds of the as-received materials; all performed with $Al_{94}Fe_3Cr_3$ alloy**

As-received material	Melt-spun alloy	Extruded material	Cold-sprayed alloy
Young's modulus, GPa	85.0 ± 2.2	72.0 ± 2.3	87.7 ± 2.5

first glance that, plasticity characteristic δ_H/δ_A of extruded material takes the smallest values despite of the most reduced microhardness, *HV*. Explanation of this is the fact that plasticity is also controlled by Young's modulus besides microhardness, as evidenced from Equation (1) used for calculation of the characteristic δ_H (see section 2). The results of mechanical testing show that Young's modulus for as-extruded material is the smallest compared to both as-spun alloy and as-received cold-sprayed alloy, as can be seen in Table 2.

Of importance is the fact that Young's modulus decreases sharply down to $E = 66 \pm 2.3$ GPa as heat treatment temperature tends to increase up to the temperature of 600 °C when all kinds of the $Al_{94}Fe_3Cr_3$ alloy demonstrate the same microstructure composed of crystalline particles of the stable θ-phases embedded in α-Al matrix.

It is essential that plasticity characteristic δ_H/δ_A of the quasi-crystalline $Al_{94}Fe_3Cr_3$ alloy fabricated by different technique including melt-spinning, hot-extrusion, and cold-spraying is just below critical value, $\delta_H \geq 0.9$, which is presently considered as criterion of ductile behaviour of metals and alloys in conventional tests by tensile and bending [77]. It was published earlier that ductile behaviour is indicative of atomized powder, which gives plasticity characteristic about $\delta_H/\delta_A \approx 0.92$, ensuring its good deformability under consolidation and, hence, making bulk-shaped material [71]. Thus, all of the processing routes are thought to be potentially suitable for performance of the quasi-crystalline structure for the $Al_{94}Fe_3Cr_3$ alloy, which demonstrates high strength and rather high ductility sufficient with respect to damage tolerance. However, powder atomization technique is thought to be preferable compared to rapid solidification by melt spinning not only from the standpoint of mass production but also for making of bulk-shaped material. In addition, as applied to structural performance of the ternary Al–Fe–Cr alloy cold spraying offers essential advantages as compared to currently employed hot extrusion. The main benefit concerns the fact that fraction volume of quasi-crystalline particles indicative of the feedstock atomized powder remains at the most in the microstructure of the as-sprayed alloy, providing superior combination of high strength and sufficient ductility of material. Of importance remark is that the as-received cold-sprayed material based on $Al_{94}Fe_3Cr_3$ alloy exhibit the value of hardness higher by roughly 20% than that for commercial 2618 aluminium alloy (Al–Cu–Mg–Fe–Ni). The value of Vickers hardness normally obtained for cast 2618 alloy after ageing at the peak T6 condition is about 1.45 GPa [91] while that for the cold-sprayed alloy aged at the same condition was found to be even slightly higher [86]. Apart from, the cold-sprayed $Al_{94}Fe_3Cr_3$ alloy demonstrates thermal stability of the structure and, hence, mechanical properties at least up to the temperature of 350 °C, suggesting its competitiveness to 2618 Al alloy recom-

mended for application under intermediate temperatures (≈230 °C) and successfully used in aircraft industry [92].

4. Conclusions

Crucial role of processing route in term of its effect on structural performance, heat treatment response, and mechanical properties of the nano-quasi-crystalline $Al_{94}Fe_3Cr_3$ alloy was justified. Several processes including melt spinning, water atomized technique were used to perform the quasi-crystalline $Al_{94}Fe_3Cr_3$ alloy in form of semi-products such as rapidly solidified ribbons and atomized powder while hot extrusion and cold spraying were employed to fabricate bulk-shaped materials including extruded rods and thick coatings respectively. Essential differences in microstructure and mechanical behaviour for the different kinds of the nano-quasi-crystalline $Al_{94}Fe_3Cr_3$ alloy were found and specified.

As applied to semi-products, the main difference is that a number of nanosize quasi-crystals of icosahedral phase (*i*-phase) embedded in α-Al matrix are found in the microstructure of the as-atomized powder, whereas the grain boundary precipitates and very small particles of the metastable crystalline $Al_{13}(Fe,Cr)_{2–4}/Al_6Fe$ phases inside the α-Al grains are formed additionally in the microstructure of the as-spun alloy. In addition, dislocation density recorded in α-Al solid solution of the as-atomized powder achieves the value about $\rho = 10^{13}$ m/m^3 while that of the as-spun alloy was found to be less by 2 order magnitude the same as for many other cast metals and alloys.

Consolidation of the atomized powder in bulk-shaped materials brings essential differences in microstructure of the quasi-crystalline $Al_{94}Fe_3Cr_3$ alloy. Powder compact degassing at the elevated temperature of 350 °C for 1 hour, which is implemented prior hot extrusion, favours partial dissolution of nanosize quasi-crystalline particles together with creation of more stable crystalline particles of the Al_6Fe-phase. Cold-spraying offers essential advantages in retaining quasi-crystalline particles presented in the feedstock powder since adiabatic increase of temperature resulted from strong impact during ultrashort time results in dissolution of the quasi-crystals located only at the particle/particle interface while the other quasi-crystals placed inside powder particles remain intact. In addition, dislocation density in heavily deformed structure of the as-sprayed alloy increases up to 10^{15} m/m^3 while that observed in deformation-induced structure of the extruded material achieves the value of 10^{16} m/m^3.

Evolution of the nanocrystalline $Al_{94}Fe_3Cr_3$ alloy in response to heat treatment was found to be strictly dependent on structural features of the as-received material and, in turn, on processing strategy. The presence of the ultrafine crystalline precipitates promotes formation of big

in size crystalline particles of the metastable Al_6Fe phase in the microstructure of the as-spun alloy at the heat temperature lower by 50 °C than that observed for the $Al_{94}Fe_3Cr_3$ alloy produced by the other processing routes. Dislocation activity in heavily deformed structure of the as-extruded material and the as-sprayed alloy offers increased kinetic of the quasi-crystalline particles decomposition and simultaneous formation of crystalline phases due to facilitated dissolution of alloyed elements in α-Al matrix, resulting in shift of the above phase transformation peak by 50 °C toward smaller temperatures compared to the feedstock-atomized powder.

Mechanical properties for the all kinds of $Al_{94}Fe_3Cr_3$ alloy fabricated by different processing routes were examined and analysed. A set of mechanical characteristics including microhardness, *HV*, yield stress, σ_y, Young's modulus, *E*, and plasticity characteristic δ_H/δ_A was determined by using indentation technique. Mechanical behaviour for the all kinds of the $Al_{94}Fe_3Cr_3$ alloy in response of heat treatment was clarified by considering classical strengthening mechanisms of structure. It was justified that nanosize quasi-crystalline particles of *i*-phase play crucial role in performance superior combination of high strength and sufficient ductility. In line with this cold-spraying technique offers essential advantage in structural performance of bulk-shaped material based on the ternary Al–Fe–Cr alloy. Strength properties (*HV*, σ_y, *E*) and plasticity characteristic (δ_H/δ_A) of the cold-sprayed $Al_{94}Fe_3Cr_3$-alloy have much higher values than those provided by currently employed hot extrusion. Despite of plasticity characteristic (δ_H/δ_A) for the $Al_{94}Fe_3Cr_3$ alloy is just below critical value $\delta_H \geq 0.9$, which was indicated as criterion of material ductile behaviour in conventional tensile and bending tests, it is rather high and sufficient for workability with respect to damage tolerance. In any way, the cold-sprayed $Al_{94}Fe_3Cr_3$ alloy kept almost stable values of mechanical properties at least up to 350 °C. Because of this, the cold-sprayed $Al_{94}Fe_3Cr_3$ alloy could be considered as competitiveness candidate to commercial Al alloys recommended for application in engineering practice under intermediate temperature.

The results of this work bring a better understanding of the interplay between processing strategy, microstructure, heat treatment response, and mechanical behaviour of the Al–Fe–Cr based alloy.

Acknowledgment. The authors are obliged to Dr. V.S. Voropaev for the help with performance of extruded rods and Mr. V.V. Kuprin for making the melt-spun ribbons.

REFERENCES

1. M.-G. Barthes-Labrousse and J.-M. Dubois, *Philos. Mag.*, **88**, Nos. 13–15: 2217 (2008).
   https://doi.org/10.1080/14786430802023036
2. J.-M. Dubois, E. Belin-Ferré, and M. Feuerbacher, *Complex Metallic Alloys: Fundamentals and Applications* (Eds. J.-M. Dubois and E. Belin-Ferré) (Weinheim: Wiley-Vch Verlag: 2011), p. 1.
3. J.-M. Dubois, *Chem. Soc. Rev.*, **41**, No. 20: 6760 (2012).
   https://doi.org/10.1039/C2CS35110B
4. D. Shechtman, I. Blech, D. Gratias, and J.W. Cahn, *Phys. Rev. Lett.*, **53**, No. 20: 1951 (1984).
   https://doi.org/10.1103/PhysRevLett.53.1951
5. D. Shechtman and I.A. Blech, *Metall. Trans. A*, **16**, No. 6: 1005 (1985).
   https://doi.org/10.1007/BF02811670
6. L. Bendersky, *Phys. Rev. Lett.*, **55**, No. 14: 1461 (1985).
   https://doi.org/10.1103/PhysRevLett.55.1461
7. A.-P. Tsai, A. Inoue, and T. Masumoto, *Jpn. J. Appl. Phys.*, **26**, No. 9: L1505 (1987).
   https://iopscience.iop.org/article/10.1143/JJAP.26.L1505/meta
8. A.-P. Tsai, A. Inoue, and T. Masumoto, *Mater. Trans., JIM*, **30**: 463 (1989).
   https://doi.org/10.2320/matertrans1989.30.463
9. Z.M. Stadnik, *Physical Properties of Quasicrystals* (Berlin: Springer-Verlag: 1999).
10. L.I. Adeeva and A.L. Borisova, *Phys. Chem. Solid St.*, **3**, No. 3: 454 (2002) (in Russian).
11. S Takeuchi, *Quasicrystals* (Tokyo: Sangyo Tosho: 1993), p. 125.
12. J.-M. Dubois, *An Introduction to Structure, Physical Properties and Application of Quasicrystalline Alloys* (Eds. J.-B. Suck, M. Schreiber, and P. Hausler) (Berlin: Springer Verlag: 1998), p. 392.
13. H Tanaka and T. Fujiwara, *Structure and Properties of Aperiodic Materials* (Eds. Y. Kawazoe, Y. Waseda) (Berlin: Springer-Verlag: 2003) p. 1.
14. E. Hornbogen and M. Shandl, *Mater. Res. Adv. Tech.*, **83**, No. 2: 128 (1992).
15. J.-M. Dubois, S.S. Kang, and Y. Massiani, *J. Non Cryst. Solids*, **153–154**: 443 (1993).
    https://doi.org/10.1016/0022-3093(93)90392-B
16. S.S. Kang, J.M. Dubois, and J. von Stebut, *J. Mater. Res.*, **8**, No. 10: 2471 (1993).
    https://doi.org/10.1557/JMR.1993.2471
17. K. Urban, M. Feuerbacher, and M. Wollgarten, *MRS Bull.*, **22**, No. 11: 65 (1997).
    https://doi.org/10.1557/S0883769400034461
18. A. Rüdiger and U. Köster, *Mater. Sci. Eng. A*, **294–296**: 890 (2000).
    https://doi.org/10.1016/S0921-5093(00)01037-6
19. J.-M. Dubois, P. Brunet, W. Costin, and A. Merstallinger, *J. Non-Cryst. Solids*, **334–335**: 475 (2004).
    https://doi.org/10.1016/j.jnoncrysol.2003.12.027
20. S. Polishchuk, P. Boulet, A. Mézin, M.-C. de Weerd, S. Weber, J. Ledieu, J.-M. Dubois, and V. Fournée, *J. Mater. Res.*, **27**, No. 5: 837 (2012).
    https://doi.org/10.1557/jmr.2011.415

21. J.-M. Dubois, S. S. Kang, and J. Von Stebut, *J. Mater. Sci. Lett.*, **10**, No. 9: 537 (1991).
https://doi.org/10.1007/BF00726930
22. J.E. Shield, J.A. Campbell, and D.J. Sordelet, *J. Mater. Sci. Lett.*, **16**, No. 24: 2019 (1997).
https://doi.org/10.1023/A:1018544313643
23. M.F. Besser and T. Eisenhammer, *MRS Bull.*, **22**, No. 11: 59 (1997).
https://doi.org/10.1557/S088376940003445X
24. T. Duguet, V. Fournée, J.-M. Dubois, and T. Belmonte, *Surf. Coat. Technol.*, **205**, No. 1: 9 (2010).
https://doi.org/10.1016/j.surfcoat.2010.05.030
25. L. Aloui, T. Duguet, F. Haidara, M.-C. Record, D. Samélor, F. Senocq, D. Mangelinck, and C. Vahlas, *Appl. Surf. Sci.*, **258**, No. 17: 6425 (2012).
https://doi.org/10.1016/j.apsusc.2012.03.053
26. A. Inoue, M. Watanabe, H.M. Kimura, F. Takahashi, A. Nagata, and T. Masumoto, *Mater. Trans. JIM,* **33**, No. 8: 723 (1992).
http://doi.org/10.2320/matertrans1989.33.723
27. A. Inoue, *Nanostruct. Mater.*, **6**, Nos. 1–4: 53 (1995).
https://doi.org/10.1016/0965-9773(95)00029-1
28. A. Inoue, *Prog. Mater. Sci.*, **43**, No. 5: 365 (1998).
https://doi.org/10.1016/S0079-6425(98)00005-X
29. D.J. Sordelet, M.F. Besser, and J.L. Logsdon, *Mater. Sci. Eng. A*, **255**, Nos. 1–2: 54 (1998).
https://doi.org/10.1016/S0921-5093(98)00778-3
30. X. Guo, G. Zhang, W. Li, Y. Gao, H. Liao, and C. Coddet, *Appl. Surf. Sci.*, **255**, No. 6: 3822 (2009).
https://doi.org/10.1016/j.apsusc.2008.10.041
31. B.N. Mordyuk, M.O. Iefimov, K.E. Grinkevych, A.V. Sameljuk, and M.I. Danylenko, *Surf. Coat. Technol.*, **205**, Nos. 23–24:5278 (2011).
https://doi.org/10.1016/j.surfcoat.2011.05.046
32. X. Guo, J. Chen, H. Yu, H. Liao, and C. Coddet, *Surf. Coat. Technol.*, **268**: 94 (2015).
https://doi.org/10.1016/j.surfcoat.2014.05.062
33. T.J. Watson, A. Nardi, A.T. Ernst, I. Cernatescu, B.A. Bedard, and M. Aindow, *Surf. Coat. Technol.*, **324**: 57 (2017).
https://doi.org/10.1016/j.surfcoat.2017.05.049
34. A. Inoue and H. Kimura, *Nanosruct. Mater.*, **11**, No. 2: 221 (1999).
https://doi.org/10.1016/S0965-9773(99)00035-5
35. A. Inoue and H. Kimura, *Mater. Sci. Eng. A,* **286**, No. 1: 1 (2000).
https://doi.org/10.1016/S0921-5093(00)00656-0
36. F. Audebert, F. Prima, M. Galano, M. Tomut, P.J. Warren, I.C. Stone, and B. Cantor, *Mater. Trans.*, **43**, No. 8: 2017 (2002).
https://doi.org/10.2320/matertrans.43.2017
37. Yu.V. Milman, A.I. Sirko, M.O. Iefimov, O.D. Niekov, A.O. Sharovsky, and N.P. Zacharova, *High Temp. Mater. Processes*, **25**, Nos. 1–2: 19 (2006).
https://doi.org/10.1515/HTMP.2006.25.1-2.19
38. M. Galano, F. Audebert, A. Garcна-Escorial, I.C. Stone, and B. Cantor, *Acta Mater.*, **57**, No. 17: 5120 (2009).
https://doi.org/10.1016/j.actamat.2009.07.009
39. M. Galano, F. Audebert, I. C. Stone, and B. Cantor, *Acta Mater.*, **57**: 5107 (2009).
https://doi.org/10.1016/j.actamat.2009.07.011

40. Yu.V. Milman, *Mater. Sci. Forum*, **482**: 77 (2005).
https://doi.org/10.4028/www.scientific.net/MSF.482.77
41. N.W. Khun, R.T. Li, and K.A. Khor, *Tribology Trans.*, **58**, No. 5: 859 (2015).
https://doi.org/10.1080/10402004.2015.1023411
42. M.O. Iefimov, D.V. Lotsko, Yu.V. Milman, A.L. Borisova, S.I. Chugunova, Ye.A. Astakhov, and O.D. Neikov, *High Temp. Mater. Processes*, **25**, Nos. 1–2: 31 (2006).
https://doi.org/10.1515/HTMP.2006.25.1-2.31
43. Yu.V. Milman, D.V. Lotsko, O.D. Neikov, A.I. Sirko, N.A. Yefimov, A.N. Bilous, D.B. Miracle, and O.N. Senkov, *Mater. Sci. Forum*, **396–402**: 723 (2002).
https://doi.org/10.4028/www.scientific.net/MSF.396-402.723
44. M.V. Semenov, M.M. Kiz, M.O. Iefimov, A.I. Sirko, A.V. Byakova, and Yu.V. Milman, *Nanosistemi, Nanomateriali, Nanotehnologii*, **4**, No. 4: 767 (2006) (in Russian).
45. J.M. Dubois, A. Proner, B. Bucaille, Ph. Cathonnet, C. Dong, V. Richard, A. Pianelli, Y. Massiani, S. Ait-Yaazza, and E. Belin-Ferré, *Ann. Chim. Sci. Mat.*, **19**: 3 (1994).
46. D.J. Sordelet, S.D. Widener, Y. Tang, and M.F. Besser, *Mater. Sci. Eng. A*, **294–296**: 834 (2000).
https://doi.org/10.1016/S0921-5093(00)01056-X
47. Bruno Alessandro Silva Guedes de Lima, Rodinei Medeiros Gomes, Severino Jackson Guedes de Lima, Diana Dragoe, Marie-Geneviéve Barthes-Labrousse, Richard Kouitat-Njiwa, and Jean-Marie Dubois, *Sci. Technol. Adv. Mater.*, **17**, No. 1: 71 (2016).
https://doi.org/10.1080/14686996.2016.1152563
48. T. Eisenhammer, *Thin Solid Films*, **270**, No. 1: 1 (1995).
https://doi.org/10.1016/0040-6090(95)06833-3
49. H.M. Kimura, K. Sasamori, and A. Inoue, *J. Mater. Res.*, **15**, No. 12: 2737 (2000).
https://doi.org/10.1557/JMR.2000.0392
50. M. Galano, F. Audebert, A. García-Escorial, I. C. Stone, and B. Cantor, *J. Alloys Compd.*, **495**, No. 2: 372 (2010).
https://doi.org/10.1016/j.jallcom.2009.10.208.
51. M. Galano, F. Audebert, B. Cantor, and I. Stone, *Mater. Sci. Eng. A*, **375–377**: 1206 (2004).
https://doi.org/10.1016/j.msea.2003.10.066
52. S. Pedrazzini, M. Galano, F. Audebert, D. M. Collins, F. Hofmann, B. Abbey, A.M. Korsunsky, M. Lieblich, A. Garcia Escorial, and G.D. W. Smith, *Mater. Sci. Eng. A*, **672**: 175 (2016).
https://doi.org/10.1016/j.msea.2016.07.007
53. Z. Chlup, I. Todd, A. Garcia-Escorial, M. Lieblich, A. Chlupová, and J.G. O'Dwyer, *Mater. Sci. Forum*, **426–432**: 2417 (2003).
https://doi.org/10.4028/www.scientific.net/MSF.426-432.2417.
54. N. Ott, A. Beni, A. Ulrich, C. Ludwig, and P. Schmutz, *Talanta*, **120**: 230 (2014).
https://doi.org/10.1016/j.talanta.2013.11.091
55. E. Ura-Binczyk, N. Homazava, A. Ulrich, R. Hauert M. Lewandowska, K.J. Kurzydlowski, and P. Schmutz, *Corros. Sci.*, **53**, No. 5: 1825 (2011).
https://doi.org/10.1016/j.corsci.2011.01.061.

56. A. Beni, N. Ott, E. Ura-Bińczyk, M. Rasinski, B. Bauer, P. Gille, A. Ulrich, and P. Schmutz, *Electrochim. Acta*, **56**, No. 28: 10524 (2011). https://doi.org/10.1016/j.electacta.2011.08.092
57. Y. Massiani, S. Ait Yaazza, J. P. Crousier, and J-M. Dubois, *J. Non-Cryst. Solids*, **159**, Nos. 1–2: 92 (1993). https://doi.org/10.1016/0022-3093(93)91286-C.
58. D. Veys, C. Rapin, X. Li, L. Aranda, V. Fournée, and J-M. Dubois, *J. Non-Cryst. Solids*, **347**, Nos. 1–3: 1 (2004). https://doi.org/10.1016/j.jnoncrysol.2004.09.004.
59. R.T. Li, Z.L. Dong, N.W. Khun, and K.A. Khor, *Mater. Sci. Technol.*, **31**, No. 6: 688 (2015). https://doi.org/10.1179/1743284714Y.0000000645
60. N.W. Khun, R.T. Li, K. Loke, and K.A. Khor, *Tribology Trans.*, **58**, No. 4: 616 (2015). https://doi.org/10.1080/10402004.2014.991860.
61. A. Ziani, G. Michot, A. Pianelli, A. Redjaïmia, C.Y. Zahra, and A.M. Zahra, *J. Mater. Sci.*, **30**, No. 11: 2921 (1995). https://doi.org/10.1007/BF00349664.
62. C. Zhang, Y. Wu, X. Cai, F. Zhao, S. Zheng, G. Zhou, and S. Wu, *Mater. Sci. Eng. A*, **323**, Nos. 1–2: 226 (2002). https://doi.org/10.1016/S0921-5093(01)01353-3.
63. K.N. Ishihara, S.R. Nishitani, and P.H. Shingu, *Trans. ISIJ*, **28**, No. 1: 2 (1988). http://doi.org/10.2355/isijinternational1966.28.2.
64. H. Lones, *Rep. Prog. Phys.*, **36**, No. 11: 1425 (1973). https://doi.org/10.1088/0034-4885/36/11/002
65. J. Gurland and N.M. Parih, *Fracture: An Advanced Treatise* (Ed.H. Liebowitz) (New York, USA: Academic Press, Inc: 1972), p. 841.
66. K. Urban, N. Moser, and H. Kronmüller, *Phys. Status Solidi A*, **91**, No. 2: 411 (1985). https://doi.org/10.1002/pssa.2210910209
67. C. Banjongprasert, S.C. Hogg, I.G. Palmer, N. Grennan-Heaven, I.C. Stone, and P.S. Grant, *Mater. Sci. Forum*, **561–568**: 1075 (2007). https://doi.org/10.4028/www.scientific.net/MSF.561-565.1075.
68. H.J. Kestenbach, C. Bolfarini, C.S. Kiminami, and W.J. Botta Filho, *J. Metastable Nanocryst. Mater.*, **20–21**: 382 (2004). https://doi.org/10.4028/www.scientific.net/JMNM.20-21.382
69. A. García-Escorial, E. Natale, V.J. Cremaschi, I. Todd, and M. Lieblich, *J. Alloys Compd.*, **643**: S199 (2015). https://doi.org/10.1016/j.jallcom.2014.12.164.
70. R.T. Li, Z.L. Dong, and K.A. Khor, *Scripta Mater.*, **114**: 88 (2016). https://doi.org/10.1016/j.scriptamat.2015.12.011.
71. A.V. Byakova, M.M. Kiz, A.I. Sirko, M.S. Yakovleva, and Yu.V. Milman, *High Temp. Mater. Processes*, **29**, Nos. 5–6: 325 (2010). https://doi.org/10.1515/HTMP.2010.29.5-6.325
72. S. Yin, P. Cavaliere, B. Aldwell, R. Jenkins, H. Liao, W. Li, and R. Lupoi, *Addit. Manuf.*, **21**: 628 (2018). https://doi.org/10.1016/j.addma.2018.04.017
73. O.D. Neikov, V.G. Kalinkin, A.F. Lednyansky, and G.I. Vasilieva, *Sposob Polucheniya Poroshkov Aluuminiya i Yego Splavov* [Method for Production of Al and Al-Based Alloys]: *Patent 2078427 RU*. MKI, B22F9/08 (Bul., 12) (1997) (in Russian).
74. A. Papyrin, V. Kosarev, S. Klinkov, A. Alkhimov, and V. Fomin, *Cold Spray Technology* (Ed. A. Papyrin) (Amsterdam: Elsevier Ltd.: 2007).

75. J.V. Cahn, D. Schehntman, and D. Gratias, *J. Mater. Res.*, **1**, No. 1: 13 (1986). https://doi.org/10.1557/JMR.1986.0013
76. Yu.V. Milman and S.I. Chugunova, *Int. J. Impact Eng.*, **23**, No. 1: 629 (1999). https://doi.org/10.1016/S0734-743X(99)00109-8
77. Yu.V. Milman, B.A. Galanov, and S.I. Chugunova, *Acta Metall. Mater.*, **41**, No. 9: 2523 (1993). https://doi.org/10.1016/0956-7151(93)90122-9
78. W.C. Oliver and G.M. Pharr, *J. Mater. Res.*, **7**, No. 6: 1564 (1992). https://doi.org/10.1557/JMR.1992.1564
79. Yu.V. Milman, *J. Phys. D: Appl. Phys.*, **41**, No. 7: 1 (2008). https://doi.org/10.1088/0022-3727/41/7/074013
80. Yu. Milman, S. Dub, and A. Golubenko, *Mater. Res. Soc. Symp. Proc.*, **1049**: 123 (2008). https://doi.org/10.1557/PROC-1049-AA05-06.
81. M. Grujicic, J.R. Saylor, D.E. Beasley, W.S. DeRosset, and D. Helfritch, *Appl. Surf. Sci.*, **219**, Nos. 3–4: 211 (2003). https://doi.org/10.1016/S0169-4332(03)00643-3.
82. R.C. McCune, W.T. Donlon, O.O. Popoola, and E.L. Cartwright, *J. Therm. Spray Technol.*, **9**, No. 1: 73 (2000). https://doi.org/10.1361/105996300770350087.
83. W.-Y. Li, H. Liao, C.-J. Li, G. Li, C. Coddet, and X. Wang, *Appl. Surf. Sci.*, **253**, No. 5: 2852 (2006). https://doi.org/10.1016/j.apsusc.2006.05.126.
84. H. Assadi, F. Gärtner, T. Stoltenhoff, and H. Kreye, *Acta Mater.*, **51**, No. 15:4379 (2003). https://doi.org/10.1016/S1359-6454(03)00274-X
85. M. Grujicic, C.L. Zhao, W.S. DeRosset, and D. Helfritch, *Mater. Des.*, **25**, No. 8: 681 (2004). https://doi.org/10.1016/j.matdes.2004.03.008.
86. L. Ajdelsztajn, A. Zúciga, B. Jodoin, and E.J. Lavernia, *Surf. Coat. Technol.*, **201**, No. 6: 2109 (2006). https://doi.org/10.1016/j.surfcoat.2005.06.001
87. H. El-Sobky, *Explosive Welding, Forming and Compaction* (Eds. T.Z. Blazynski) (London: Applied Science Publishers Ltd.: 1983), p. 189.
88. F. Prima, M. Tomut, I. Stone, B. Cantor, D. Janickovic, G. Vlasak, and P. Svec, *Mater. Sci. Eng. A*, **375–377**: 772 (2004). https://doi.org/10.1016/j.msea.2003.10.264.
89. N. Takata, K. Yamada, K. Ikeda, F. Yoshida, H. Nakashima, and N. Tsuji, *Mater. Sci. Forum*, **503–504**: 919 (2006). https://doi.org/10.4028/www.scientific.net/MSF.503-504.919
90. G. Benchabane, Z. Boumerzoug, I. Thibon, and T. Gloriant, *Mater. Charact.*, **59**, No. 10: 1425 (2008). https://doi.org/10.1016/j.matchar.2008.01.002
91. I.N.A. Oguocha, M. Radjabi, and S. Yannacopoulos, *J. Mater. Sci.*, **35**, No. 22: 5629 (2000). https://doi.org/10.1023/A:1004881702823
92. J. Majimel, G. Molénat, M.J. Casanove, D. Schuster, A. Denquin, and G. Lapasset, *Scr. Mater.*, **46**, No. 2: 113 (2002). https://doi.org/10.1016/S1359-6462(01)01200-3

Received 22.06.2020;
in final version, 07.10.2020

О.В. Бякова[1], *А.О. Власов*[1], *О.А. Щерецький*[2], *О.І. Юркова*[3]
[1] Інститут проблем матеріалознавства ім. І.М. Францевича НАН України, вул. Академіка Кржижановського, 3, 03142 Київ, Україна
[2] Фізико-технологічний інститут металів та сплавів НАН України, бульв. Академіка Вернадського, 34/1, 03142 Київ, Україна
[3] Національний технічний університет України «Київський політехнічний інститут імені Ігоря Сікорського», просп. Перемоги 37, 03056 Київ, Україна

РОЛЬ ТЕХНОЛОГІЧНОГО ПРОЦЕСУ В СТРУКТУРНИХ ХАРАКТЕРИСТИКАХ КВАЗИКРИСТАЛІЧНОГО СТОПУ Al–Fe–Cr

В роботі зосереджено увагу на важливості ролі технологічного підходу з точки зору його впливу на формування структури, реакції на термічне оброблення та механічну поведінку квазикристалічного стопу Al–Fe–Cr формульного складу $Al_{94}Fe_3Cr_3$. Декілька видів напівпродуктів і масивних матеріалів було виготовлено із зазначеного стопу через застосування методів швидкої кристалізації шляхом спінінґування розтопу та розпорошення порошку й консолідацію порошку в процесі гарячої екструзії та холодного газодинамічного напорошення відповідно. Всі види напівпродуктів і масивних матеріалів містили нанорозмірні квазикристалічні частинки ікосаедричної фази (*i*-фази), втілені в алюмінієву матрицю, хоча кількість квазикристалів та інші структурні параметри відрізнялися залежно від застосованого методу одержання матеріалу, зокрема порівняно з поширеним натепер методом гарячої екструзії. Використання техніки холодного газодинамічного напорошення забезпечувало значні переваги в збереженні квазикристалічних частинок, які містились у вихідному порошку. Вирішальна роль нанорозмірних квазикристалічних частинок у наданні структурних переваг матеріалу та комбінації винятково високої міцности та пластичности потрійного стопу Al–Fe–Cr було доведено шляхом дослідження еволюції механічних властивостей під впливом нагрівання. З цією метою вплив нагріву на еволюцію структури та механічних властивостей кожного виду матеріалу зі стопу $Al_{94}Fe_3Cr_3$ було досліджено й обговорено з урахуванням класичних механізмів зміцнення. В обговоренні використовували низку механічних характеристик, включаючи мікротвердість *HV*, границю плинности σ_y, модуль Юнґа *E* та характеристику пластичности δ_H/δ_A, які визначали технікою індентування. За одержаними результатами було доведено, що властивості міцности (*HV*, σ_y, *E*) та характеристика пластичности (δ_H/δ_A) матеріалу, одержаного методом холодного газодинамічного напорошення, набагато перевищували ці характеристики для матеріалу, виготовленого відповідно до методу гарячої екструзії, який застосовують натепер. Важливо, що стоп $Al_{94}Fe_3Cr_3$, одержаний за методом холодного газодинамічного напорошення, демонстрував майже стабільні величини механічних характеристик щонайменше до 350 °C, засвідчуючи можливість його потенційного застосування в інженерній практиці в умовах середніх робочих температур.

Ключові слова: квазикристали, алюмінієвий стоп, спінінґування розтопу, розпорошування порошку, холодне газодинамічне напорошення, мікроструктура, механічні властивості.